Asian Journal of Chemistry; Vol. 38, No. 5 (2026), 1333-1340

ASIAN JOURNAL OF CHEMISTRY

https://doi.org/10.14233/ajchem.2026.35689

Green Synthesis of Cobalt Oxide Nanoparticles using *Averrhoa carambola* and *Psidium guajava* Plant Extract: Characterisation and Photocatalytic Activity Treatment of Organic Dye

H.M. SHAHADAT[1,2,*,†], S. AKTER[1,†], S.A. SATHI[1,3], F. AKTER[1], T. AKTER[1], K.A. HAQUE[1], M.L. BHOWMIK[1], M.M. HASAN[1,4] and M.S. RAHAMAN[1]

[1]Research Laboratory, Department of Chemistry, Faculty of Science, Comilla University, Cumilla 3506, Bangladesh
[2]Labortory of Organometallics, Catalysis and Ordered Materials, Comilla University, Cumilla 3506, Bangladesh
[3]School of Chemistry and Molecular Bioscience, University of Wollongong, Wollongong, NSW 2560, Australia
[4]Department of Chemistry, Bangladesh University of Engineering and Technology, Dhaka-1000, Bangladesh
[†]These authors contributed equally to this work.

*Corresponding author: E-mail: msh_chem@cou.ac.bd

Received: 2 February 2026 | *Accepted*: 14 April 2026 | *Published online*: 4 May 2026 | AJC-22359

In this research, Co_3O_4 NPs were produced by combining the leaf extracts of *Averrhoa carambola* and *Psidium guajava* with $CoCl_2{\cdot}6H_2O$ as a source of cobalt. The obtained product was calcined at 550 ºC and the synthesised nanoparticles were analysed by various techniques such as Fourier transform infrared (FT-IR), X-ray diffraction (XRD), transmission electron microscope (TEM) and ultraviolet visible (UV-Vis) spectroscopy. According to XRD, the nanoparticles generated from two types of leaf extract were found to have a size in the nano range of 19.58 and 9.03 nm, respectively which also confirms the face-cantered cubic spinel structure of synthesised Co_3O_4 NPs. Besides, the FT-IR analysis confirms the functional group present in the Co_3O_4 NPs. TEM provided surface morphological studies of Co_3O_4 NPs formed in quasi-spherical shapes and irregular shaped having both spherical and square shape, respectively. From TEM, the average particle size was determined to be 26.29 and 28.90 nm using the image J program. Scanning area electron diffraction (SAED) pattern of the nanoparticle showed bright spotted ring like image which represents polycrystalline particle, which further supports the results of XRD and TEM. The diameter of SAED rings were measured using Image J Software Version 2022 and then the *d*-spacing of the crystal planes and Miller indices (*hkl*) were estimated using excel sheet which were excellent correlation with XRD data. The photocatalytic activity of the synthesised nanoparticles was evaluated by degrading methyl blue (MB) dye and a degradation of 89.81% and 90.64% were achieved (dye conc. 50 mg/L) using 5 mg/20 mL Co_3O_4 NPs for 15 min irradiation time. Maximum degradation efficiency was sought by examining the impact of change in catalyst concentration and dye concentration. The kinetics of photodegradation are consistent with a first-order model. The current study found that *A. carambola* and *P. guajava* might be employed to synthesize Co_3O_4 NPs for photo-catalytic applications, due to their eco-friendly and low-cost characteristics.

Keywords: Green synthesis, Co_3O_4 NPs, Dye degradation, Photocatalytic activity, *Averrhoa carambola*, *Psidium guajava*.

INTRODUCTION

Nanotechnology encompasses the design and engineering of materials at dimensions typically below 100 nm, where unique physico-chemical properties arise due to quantum confinement, high surface-to-volume ratios and altered electronic behaviour [1-3]. At this scale, materials exhibit distinct optical, catalytic, mechanical and biological characteristics that differ significantly from their bulk counterparts. Nanoparticles (NPs), which serve as the fundamental units of nanostructured systems, play a crucial role in tailoring these properties for specific applications [4,5]. The distinct magnetic, mechanical thermal, optical and chemical characteristics of NPs from their bulk counterparts have attracted a lot of research during the last three decades. Industrial applications of metal oxide (MO_x) NPs can be found in many areas of applied nanotechnology including batteries, gas sensors, solar cells, magnetic storage media, catalysis, rectifiers, electronics and optoelectronics [6-8].

Nanoparticles (NPs) are materials with at least one dimension below 100 nm and may exist in 0D-3D forms depending on their structure. Their small size and high surface area result in unique properties such as enhanced reactivity and tunable electronic behaviour compared to bulk materials. Transition

This is an open access journal, and articles are distributed under the terms of the Attribution 4.0 International (CC BY 4.0) License. This license lets others distribute, remix, tweak, and build upon your work, even commercially, as long as they credit the author for the original creation. You must give appropriate credit, provide a link to the license, and indicate if changes were made.

metal oxides (MO_x) exhibit diverse oxidation states and high surface activity, making them useful in catalysis, gas sensing, energy storage and magnetic applications [5,9,10]. Their large surface area also supports efficient adsorption of heavy metals and organic pollutants, while controlled synthesis allows tuning of their properties for specific applications.

Plant-mediated synthesis has emerged as a preferred route for the preparation of cobalt and cobalt oxide nanoparticles (Co_3O_4 NPs), owing to its simplicity, safety and efficiency compared to microbial methods. Phytochemicals present in the plant extracts act as both reducing and stabilising agents, enabling controlled nanoparticle formation. Various plant parts such as leaves, roots, stems, fruits and peels have been utilised, with leaf extracts being particularly effective due to their high metabolite content [11-15]. This green approach offers a rapid, cost-effective and environmentally benign alternative to conventional synthesis methods, which often involve the hazardous reagents and energy-intensive conditions [16].

Cobalt-based nanoparticles exhibit diverse structural and functional properties due to the variable oxidation states of transition metals. The growing demand for efficient environmental remediation strategies has intensified interest in Co_3O_4 NPs, particularly as semiconductor photocatalysts. Their high surface area, chemical stability and p-type semiconducting nature enhance the adsorption and degradation of organic pollutants, including toxic and non-biodegradable dyes from industrial effluents [17-19].

Several studies have demonstrated the green synthesis of Co_3O_4 NPs using plant extracts such as *Aspalathus linearis* [20], *Citrus limon* [21], *Azadirachta indica* [22], *Calotropis gigantea* [23], *Euphorbia heterophylla* L. [24], *Curcuma longa* [25], *Helianthus annuus* [26], *Moringa oleifera* [27], and *Colocasia esculenta* [28]. In present study, we report for the first time a simple and efficient green synthesis of Co_3O_4 NPs using leaf extracts of *Averrhoa carambola* and *Psidium guajava*. The plant extracts act as natural reducing and stabilising agents, enabling an eco-friendly and controlled synthesis process. The prepared nanoparticles were further evaluated for their photocatalytic efficiency in the degradation of methylene blue (MB) dye. Furthermore, compared to the conventional chemical methods, this approach avoids toxic reagents, operates under mild conditions and cost-effective, making it a sustainable alternative. The combined advantages of green synthesis and effective photocatalytic performance highlight the potential of this method for the large-scale environmental applications, particularly in the treatment of dye-contaminated wastewater.

EXPERIMENTAL

The leaves of *Averrhoa carambola* and *Psidium guajava* were collected from local area of Cumilla city of Bangladesh and authenticated by the Botanist. Analytical grade of cobalt dichloride hexahydrate ($CoCl_2{\cdot}6H_2O$), NaOH and methyl blue (MB) dye were purchased from Merck, Germany. Throughout the experimental works, deionised water was used.

Preparation of leaf extract: The collected leaves were washed through fresh tap water followed by deionised water to remove impurities. The leaves dried under air at room temperature and mechanically grinded to obtain powder form. Then 5 g of leaf of each type was mixed with 100 mL of deionised water and the mixture was heated about 1 h at 60 ºC under continuous stirring and finally filtered to obtain leaf extract.

Synthesis of Co_3O_4 NPs using leaf extract: Co_3O_4 NPs were synthesised by green method using *A. carambola* and *P. guajava* leaf extract. In both cases, same procedure was maintained where a 0.1 M, 100 mL $CoCl_2{\cdot}6H_2O$ solution was prepared. Then 10 mL of leaf extract was added in 0.1 M, 100 mL $CoCl_2$ solution under continuous stirring at 60 ºC. The mixture was stirred about 2 h at 60 ºC. The colour change was noted from light brown to deep red brown during the stirring. After cooling, the solution was maintained at pH 12 by adding NaOH solution to stabilize the nanoparticles. Then the solution was centrifuged followed by drying the centrifuged particle in oven at 120 ºC for 2 h. Finally, the obtained nanoparticles were calcined at 550 ºC for 3 h in a muffle furnace to yield phase-pure Co_3O_4 NPs, which appeared as a black solid.

Characterisation: The ultraviolet-visible spectrum was recorded using Shimadzu UV-VIS 1800 spectrometer at 200-800 nm using deionised water as a reference. FT-IR spectrum of the Co_3O_4 was recorded at the region 4000-400 cm^{-1} on Perkin-Elmer FT-IR spectrometer using KBr pellets. The sample was placed under pressure for 30 sec and a translucent pellet was formed. The IR spectrum was recorded and the crystal structure was analysed using a GNR X-ray diffractometer explorer with Cu-$K_{\alpha1}$ radiation (λ = 1.5406 Å). The samples were dried, crushed and placed in a PXRD sample container. The X-ray source was unfiltered Cu$K\alpha$ radiation (λ = 1.5418 Å) and the surface morphology was studied using transmission electron microscope spectroscopy. To prepare the nanoparticles, 1-2 mg of the synthesised nanoparticle was taken in a glass vial and 5 mL of 70% ethanol was added. The mixture was dispersed in a water bath for 2 h.

Photocatalytic degradation of methylene blue (MB) dye: The calibration curve was prepared by plotting the absorbance of known MB concentration (1-45 ppm) prepared from stock solution of 50 ppm MB dye solution. A CAMAG UV lamp was used to conduct the photocatalytic process under UV light irradiation at a wavelength of 254 nm and a power frequency of 50-60 Hz. In this investigation, 20 mL of 50 ppm MB dye solution was mixed with 5 mg in 20 mL Co_3O_4 NPs and stirred in dark for 5 min. After the completion of adsorption, UV light was applied to the suspension for 15 min. Due to the presence of Co_3O_4 NPs, MB dye was degraded and turns into a colourless solution. The absorbance of MB dye solution was monitored at predetermined intervals.

RESULTS AND DISCUSSION

The formation of Co_3O_4 NPs was initially indicated by a distinct colour change from light brown to deep reddish-brown, suggesting successful reduction and nucleation mediated by the leaf extract. This preliminary observation was further validated through comprehensive characterisation using FT-IR, XRD, UV-Vis spectroscopy and TEM analyses, confirming the successful synthesis of the desired Co_3O_4 NPs.

FT-IR spectral studies: FT-IR spectra of Co_3O_4 NPs synthesised from *A. carambola* and *P. guajava* leaf extract are shown in Fig. 1a-b. The synthesised Co_3O_4 NPs from *A.*

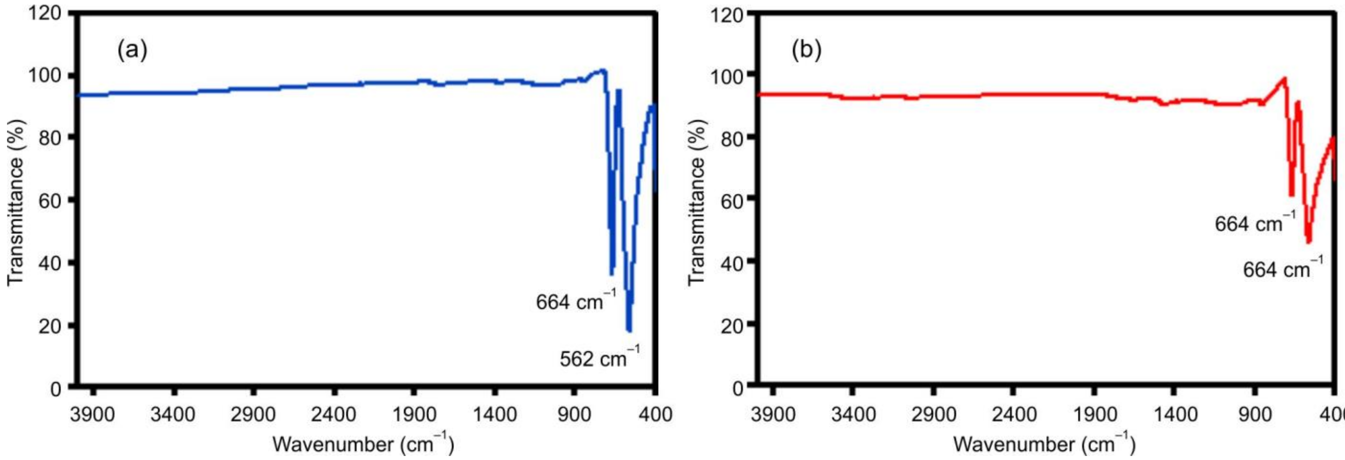

Fig. 1. FT-IR spectra of Co_3O_4 NPs synthesised using *Averrhoa carambola* (a) and *Psidium guajava* (b) leaf extracts

carambola displayed a significant absorption peak at 562 and 664 cm^{-1}. The formation of spinel Co_3O_4 NPs was confirmed by the absorption band at 664 cm^{-1}, which corresponded to ABO_3 type and represented the Co^{2+} ions in the tetrahedral positions. The band at 562 cm^{-1} was imposed to Co-O vibrations in octahedral sites of OB_3 type, where B represents Co^{3+} ions in the octahedral site. The absence of any other peak indicates that only pure NPs were formed [29-31]. However, Co_3O_4 NPs from *P. guajava* leaf extract exhibited a significant absorption peak at 564 and 664 cm^{-1}. The absorption band at 564 cm^{-1} was assigned to Co-O stretching vibration mode and the band at 664 cm^{-1} corresponded to the bridging vibration O-Co-O bond [32,33].

XRD studies: The synthesised Co_3O_4 NPs were characterised by X-ray diffraction (XRD) system. The XRD data was analysed by Origin Pro Graphing and Analysis 2018 software for getting the crystallite size and the final product obtained by green synthesis as shown in Fig. 2a-b, respectively. For Co_3O_4 NPs synthesised from *A. carambola*, the peak positions were 19.174º (111), 31.267º (220), 36.895º (311), 38.464º (222), 44.869º (400), 55.758º (422), 59.420º (511), 65.306º (440) and relative intensities obtained match with the JCPDS card no. 00-042-1467 file, identifying it as Co_3O_4 NPs with a cubic structure. No obvious peaks indicative of impurities was detected. The average crystallite size was determined using Debye-Scherrer's formula of the following:

$$D = \frac{k\lambda}{\beta\cos\theta} \tag{1}$$

where D is the particle size, β is the full width at half maximum of diffraction angle in radian (FWHM); θ is the scattering angle; λ is the X-ray wavelength of radiation with 1.54 Å and k is the correction factor (0.9).

The lattice parameter (a_o) determined according to the relation $a_o = d_{hkl}(h^2 + k^2 + l^2)^{1/2}$ and a_o of Co_3O_4 NPs was calculated as 8.101 Å from the major (311) plane for 36.895º diffraction peak. The average crystallite size was found to be around 19.58 nm [32,34]. In Fig. 2b, the XRD pattern disclosed eight diffraction peaks at the 2θ values of 19.040º (111), 31.399º (220), 36.924º (311), 38.422º (222), 45.049º (400), 55.853º (422), 59.645º (511) and 65.341º (440). The average crystallite size of Co_3O_4 NPs was determined using Scherrer relation and it was found to be around 19.58 nm and 9.03 nm, respectively.

TEM and SAED analysis: TEM image in Fig. 3a showed that the synthesised product possesses polycrystalline morphology. The large-area TEM picture reveals that just a small fraction of the NPs has clumped together. It can be seen that most of the NPs are quasi-spherical shaped and size estimated from the TEM images lies in the range of about 12.00-51.20 nm with average size 26.29 nm [29]. Crystallite size was estimated from XRD data by analysing the broadening of Bragg diffraction peaks. However, since a single particle may consist of multiple crystallites, XRD often provides a lower estimate compared to actual particle size. TEM image from *P. guajava* leaf extract (Fig. 3b) revealed that the Co_3O_4 NPs are predominantly irregular in morphology, comprising both

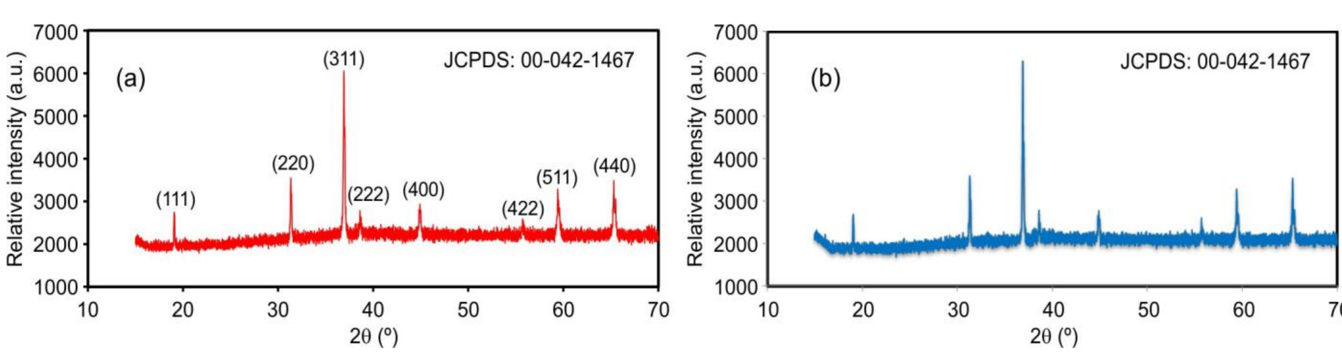

Fig. 2. XRD spectra of Co_3O_4 NPs synthesised from *Averrhoa carambola* (a) and *Psidium guajava* (b) leaf extracts

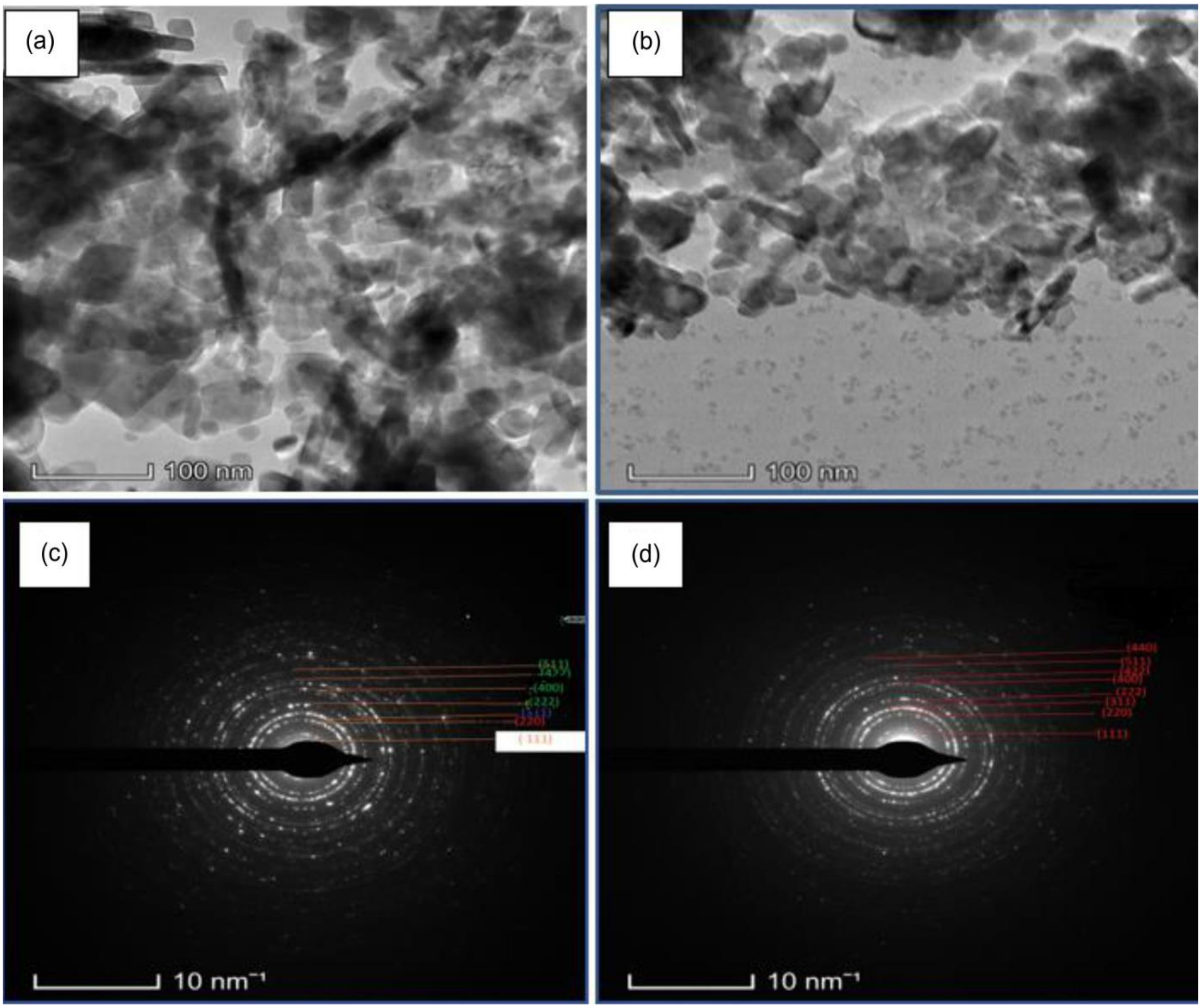

Fig. 3. TEM images of synthesised Co_3O_4 NPs using *Averrhoa carambola* (a) and *Psidium guajava* (b) leaf extracts. SAED patterns of synthesised Co_3O_4 NPs using *Averrhoa carambola* (c) and *Psidium guajava* (d) leaf extracts

spherical and quasi-square shapes, with sizes ranging from 15.15 to 46.25 nm and an average particle size of 28.90 nm [29]. The SAED pattern exhibited distinct bright concentric rings, indicative of the polycrystalline nature of the nanoparticles. This observation is in good agreement with the XRD and TEM results (Fig. 3c-d), confirming the crystalline structure of the synthesised nanoparticles.

UV-Vis studies: The UV-Vis spectra of Co_3O_4 NPs synthesised using *A. carambola* (Fig. 4a) and *P. guajava* (Fig. 4b) leaf extracts exhibited characteristic absorption bands. For *A. carambola*, two prominent peaks were observed at ~340 nm and ~620 nm, whereas *P. guajava*-mediated Co_3O_4 NPs showed bands at ~340, ~580 and ~620 nm.

The absorption in the UV region (~340 nm) is attributed to $O^{2-} \rightarrow Co^{2+}$ charge transfer transitions, while the bands in the visible region (~580-620 nm) correspond to $O^{2-} \rightarrow Co^{3+}$ charge transfer processes. These transitions confirm the formation of spinel Co_3O_4 and its p-type semiconducting nature [35].

Band gap analysis: Fig. 5 illustrates the optical band gap analysis of Co_3O_4 NPs synthesised using leaf extracts from *A. carambola* and *P. guajava*, utilizing the Tauc's plot method. The band gap energies were determined from the linear region of the Tauc plot, specifically $(\alpha h\nu)^2$ *versus* photon energy, yielding values of 2.48 eV for sample (a) and 2.49 eV for sample (b). This linear extrapolation confirms the presence of a direct allowed transition in both samples. These results indicate consistent optical properties and support the semiconducting nature of the synthesised Co_3O_4 NPs [36].

Photocatalytic degradation of methylene blue (MB) dye: The photocatalytic performance of the synthesised Co_3O_4 NPs was evaluated through the degradation of methylene blue (MB) dye under UV irradiation (Fig. 6a-b). The pristine MB solution exhibited a characteristic absorption maximum at ~590 nm. Upon UV exposure in the absence of catalyst, no significant degradation of MB was observed. In contrast, the presence of Co_3O_4 NPs (5 mg/20 mL of 50 mg/L MB solution) resulted in rapid and efficient dye degradation within 15 min.

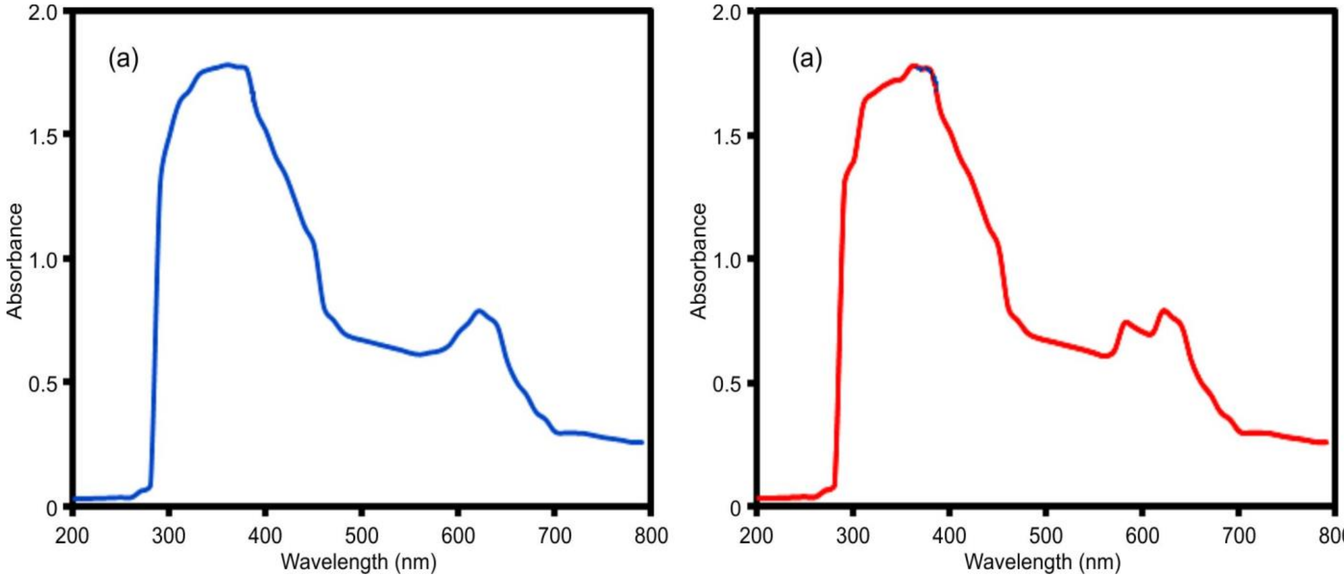

Fig. 4. UV-Vis spectra of Co_3O_4 NPs synthesised using *Averrhoa carambola* (a) and *Psidium guajava* leaf extract (b)

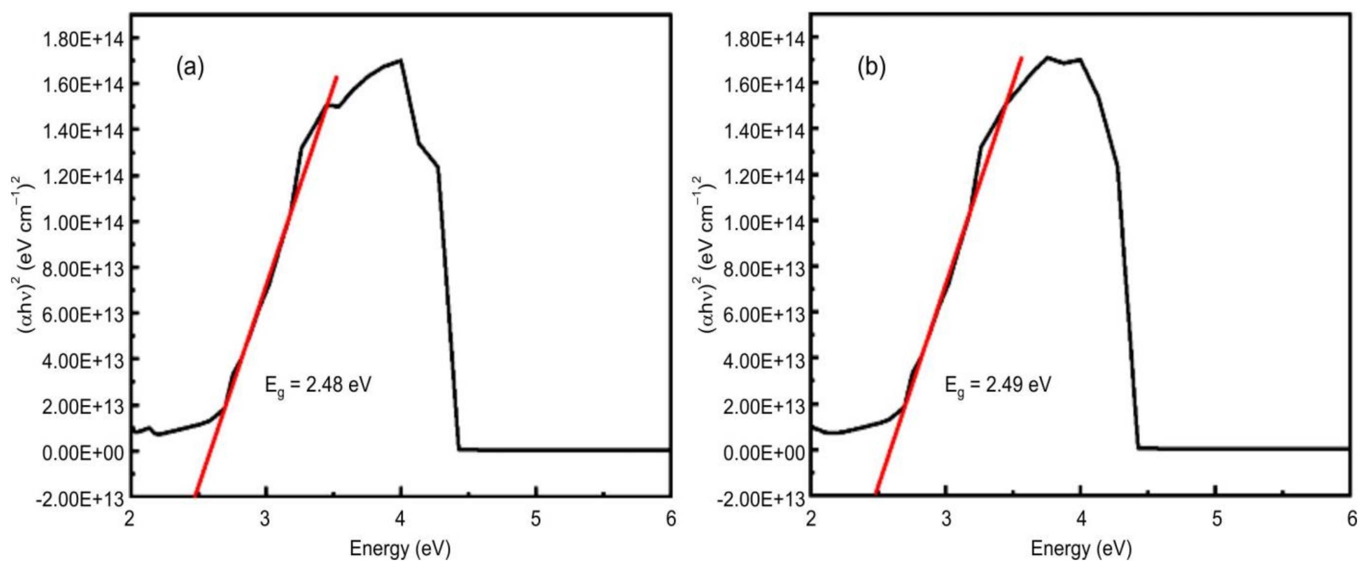

Fig. 5. Optical band gap analysis of Co_3O_4 NPs synthesised using leaf extracts from (a) *Psidium guajava* and (b) *Averrhoa carambola*

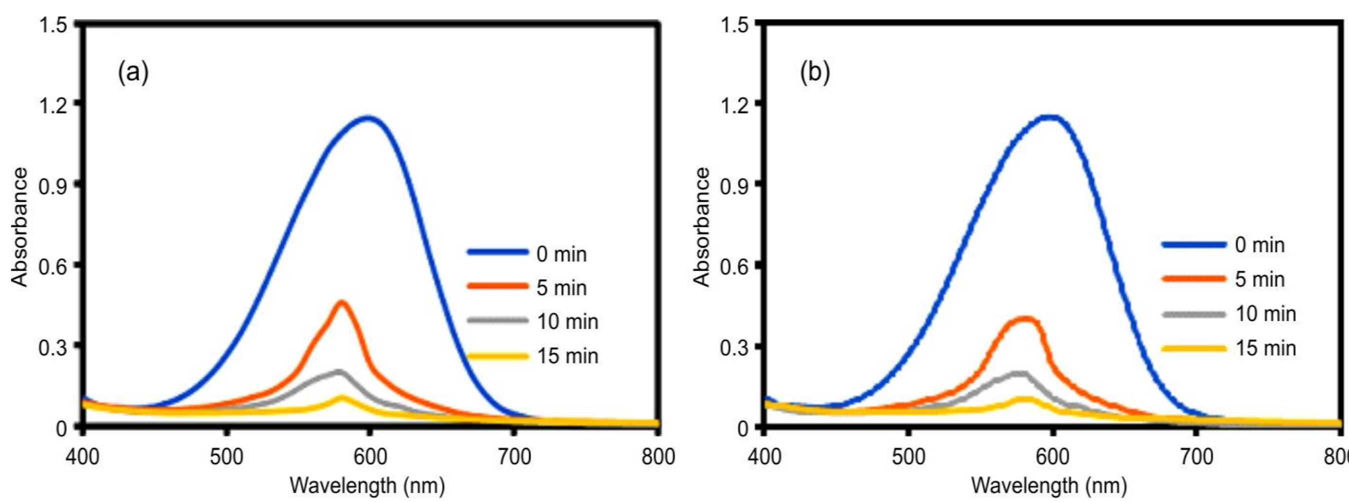

Fig. 6. UV-Vis spectra of MB dye before and after the treatment using Co_3O_4 NPs as a photocatalyst synthesised from *Averrhoa carambola* leaf extract (a) and *Psidium guajava* leaf extract (b)

Approximately 89.81% degradation was achieved using Co_3O_4 NPs using *A. carambola*, while *P. guajava*-mediated Co_3O_4 NPs showed slightly higher efficiency (90.64%). The degradation process was monitored by recording the decrease in absorbance at regular intervals using a calibration curve of methylene blue. A gradual decline in absorption intensity with increasing irradiation time confirmed the progressive breakdown of the dye molecules. The reduction in peak intensity at the maximum wavelength indicates effective decolourisation and degradation under the applied conditions. After 15 min of UV irradiation, the dye was nearly completely degraded. The photocatalytic process is expected to yield mineralisation products such as CO_2, H_2O, NH_4^+/NO_3^-, SO_4^{2-} and Cl^-.

The degradation efficiency and corresponding absorbance values are summarised in Table-1, while the comparative analysis with previously reported green-synthesised Co_3O_4 NPs is presented in Table-2, highlighting the effectiveness of the present system.

The degradation efficiency (in terms of %) has been calculated as:

$$\text{Efficiency (\%)} = \left(1 - \frac{C}{C_o}\right) \times 100 \qquad (2)$$

where C_o is the starting concentration of dye and C is the final concentration after irradiation.

Effect of concentration on photodegradation of MB dye: The study investigates the photocatalytic degradation of MB dye in aqueous suspension of Co_3O_4 NPs at varying concentrations of 10 to 70 mg/L for 15 min (Fig. 7a). The results indicate that the percentage degradation decreases with increasing dye concentration. At higher concentrations, more dye molecules compete for limited active sites on the catalyst surface, while the generation of reactive species becomes insufficient to effectively degrade all dye molecules. Also, increased dye concentration leads to greater absorption of UV light by the dye itself, thereby reducing the light available for catalytic activation and lowering overall efficiency [37,38].

The effect of photocatalyst loading on MB degradation revealed that the degradation rate increases with increasing Co_3O_4 NPs concentration from 5 to 10 mg, primarily due to the availability of more active surface sites. However, beyond this optimum level, no significant improvement in degradation was observed. This is attributed to reduced light penetration caused by increased turbidity of the suspension, which limits photon absorption and consequently decreases photocatalytic efficiency [38,39].

Kinetic study: According to the results of the kinetics of photocatalytic degradation of MB under ideal conditions, the photodegradation of an aqueous solution of MB dye in the presence of Co_3O_4 NPs under UV light can be explained by a first-order kinetic model:

$$\ln\left(\frac{C_o}{C}\right) = kt \qquad (3)$$

where C is the concentration at time t and C_o is the initial concentration.

The logarithmic plot of concentration data *vs.* time provides a straight line. The fitted line shows a correlation constant (R^2) of 0.9999 for the synthesised Co_3O_4 NPs. The rate constant was calculated to be 0.1752 min^{-1} [38].

TABLE-1
ABSORPTION AND DEGRADATION DATA OF METHYLENE BLUE DYE IN THE PRESENCE OF Co_3O_4 NPs SYNTHESISED USING *Averrhoa carambola* and *Psidium guajava* PLANT EXTRACTS

Time (min)	*Averrhoa carambola* plant extract		*Psidium guajava* plant extract	
	Absorbance	Degradation (%)	Absorbance	Degradation (%)
Initial	1.133	—	1.133	—
5	0.460	57.42	0.400	62.96
10	0.200	81.48	0.199	81.58
15	0.110	89.81	0.101	90.6

TABLE-2
COMPARATIVE EVALUATION OF PHOTOCATALYTIC DYE DEGRADATION OF METHYLENE BLUE DYE USING BIOGENIC Co_3O_4 NPs SYNTHESISED FROM DIFFERENT BIOLOGICAL SOURCES

Plant	Dose		Light source	Degradation		Ref.
	Catalysis	Dye		Time (min)	%	
Euphorbia heterophylla L. leaves	3 mg	25 mL of MB (2×10^{-5} M)	Visible light	180	63.105	[24]
Curcuma longa leaf extract	10 mg	100 mL of MB (10 mg/L)	UV light (Xenon lamp wavelength = 400 nm)	40	90	[25]
Helianthus annuus leaf extract	10 mg	50 mL of methyl orange (100 mg/L)	A 100 W incandescent light bulb	120	53	[26]
Moringa oleifera Leaves Extract	–	MB	Visible light	120	91	[27]
Colocasia esculent leaf extract	5 g	MB (20 mg/L)	UV light 300 W Xe lamp (120 μW/cm^2)	90	86.40	[28]
Averrhoa carambola and *Psidium guajava* plant extract	5 mg	20 mL of MB (50 mg/L)	CAMAG UV lamp with a wavelength of 254 nm and a power frequency of 50/60 Hz	15	89.81 and 90.64	Present study

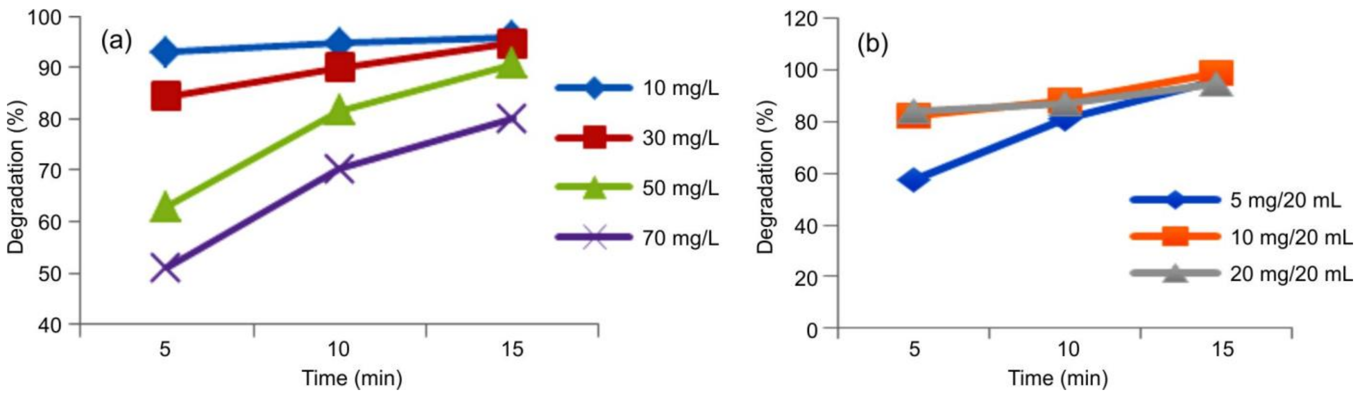

Fig. 7. Effect of methylene blue dye concentration at optimum catalyst concentration (a) and catalyst concentration at constant dye concentration (b)

Mechanism for the degradation of dye: Upon light irradiation, electrons in Co_3O_4 NPs are excited from the valence band to the conduction band, generating electron–hole pairs. The photogenerated electrons react with adsorbed oxygen to form superoxide radical anions ($O_2^{\bullet-}$), while the holes interact with water or surface hydroxyl groups to produce hydroxyl radicals ($^{\bullet}OH$). These highly reactive species attack methylene blue (MB) molecules, leading to their oxidative degradation into simpler, less harmful products. The proposed mechanism for dye degradation is outlined as follows:

$$Co_3O_4 + h\nu \rightarrow h^+ + e^- \quad \text{(Step-I)}$$

$$O_2 + e^- \rightarrow O_2^{\bullet-} \quad \text{(Step-II)}$$

$$h^+ + H_2O \rightarrow H^+ + OH^{\bullet} \quad \text{(Step-II)}$$

$$O_2^{\bullet-} + e^- + 2H^+ \rightarrow H_2O_2 \quad \text{(Step-III)}$$

$$H_2O_2 + e^- \rightarrow OH^- + OH^{\bullet} \quad \text{(Step-IV)}$$

$$OH^{\bullet} + MYB^{\bullet} \rightarrow \text{Degradation products} \quad \text{(Step-V)}$$

Conclusion

Co_3O_4 NPs were successfully synthesised by eco-friendly green synthesis using *A. carambola* and *P. guajava* plant extract. The FT-IR study confirmed Co_3O_4 NPs formation with the presence of strong M-O peaks at 562, 664 and 564, 664 cm^{-1}, respectively for Co_3O_4 (*A. carambola*) and Co_3O_4 (*P. guajava*) NPs. Co_3O_4 (*A. carambola*) and Co_3O_4 (*P. guajava*) NPs showed excellent absorption peaks at 340, 620 and 340, 580, 620 nm wavelength ranges, respectively. The XRD pattern was consistent with JCPDS card no. 00-042-1467 which confirms the cubic spinel structure of Co_3O_4 NPs. The average crystallite size of synthesised NPs was 19.58 and 9.03 nm, respectively. The average particle size was found to be 26.29 and 28.90 nm, respectively from the TEM image estimated by image J software. The SAED patterns of the Co_3O_4 NPs displayed bright spotted ring like image which correspond that the synthesised nanoparticle is a polycrystalline. Co_3O_4 NPs, synthesised using leaf extracts from *P. guajava* and *A. carambola*, exhibit direct band gaps of 2.48 eV and 2.49 eV, respectively. Co_3O_4 NPs showed effective degradation efficiency for MB dye under UV-light. The synthesised Co_3O_4 (*A. carambola*) and Co_3O_4 (*P. guajava*) NPs catalyst allowed 89.81% and 90.64% dye removal within 15 min under UV-light irradiation. The effect of experimental parameters such as catalyst concentration, dye concentration was studied in order to achieve maximum degradation efficiency. The photodegradation of aqueous solution of MB dye in the presence of Co_3O_4 NPs under UV-light follow first-order kinetic model.

ACKNOWLEDGEMENTS

The authors gratefully acknowledge the financial support provided by Comilla University, Bangladesh. One of the authors, HMS also thanks the Laboratory of Organometallics, Catalysis & Ordered Materials (LOCOM) for research support. Additional facilities and logistical assistance from the Atomic Energy Centre, Dhaka and the Wazed Miah Science Research Centre, Jahangirnagar University, Bangladesh are sincerely appreciated.

CONFLICT OF INTEREST

The authors declare that there is no conflict of interests regarding the publication of this article.

DECLARATION OF AI-ASSISTED TECHNOLOGIES

During the preparation of this manuscript, the authors used an AI-assisted tool(s) to improve the language. The authors reviewed and edited the content and take full responsibility for the published work.

REFERENCES

1. K.J. Hughes, M. Ganesan, R. Tenchov, K.A. Iyer, K. Ralhan, L.L. Diaz, R.E. Bird, J. Ivanov and Q.A. Zhou, *ACS Omega*, **10**, 7530 (2025); https://doi.org/10.1021/acsomega.4c10929
2. M. Singh, R. Kalaivani, S. Manikandan, N. Sangeetha and A. Kumaraguru, *Appl. Nanosci*., **3**, 145 (2013); https://doi.org/10.1007/s13204-012-0115-7
3. M.A. Albrecht, C.W. Evans and C.L. Raston, *Green Chem*., **8**, 417 (2006); https://doi.org/10.1039/b517131h
4. N. Baig, I. Kammakakam and W. Falath, *Mater. Adv*., **2**, 1821 (2021); https://doi.org/10.1039/D0MA00807A
5. N. Zikalala, K. Matshetshe, S. Parani and O.S. Oluwafemi, *Nano-Struct. Nano-Objects*, **16**, 288 (2018); https://doi.org/10.1016/j.nanoso.2018.07.010
6. J. Calvache-Muñoz, F.A. Prado and J.E. Rodríguez-Páez, *Colloids Surf. A Physicochem. Eng. Asp*., **529**, 146 (2017); https://doi.org/10.1016/j.colsurfa.2017.05.059
7. M.S. Chavali and M.P. Nikolova, *SN Appl. Sci*., **1**, 607 (2019); https://doi.org/10.1007/s42452-019-0592-3

8. A. Das, S.D. Peu, M.S. Hossain, M.A.M. Akanda, M.M. Salah, M.M.H. Akanda, M. Rahman and B.K. Das, *Nanomaterials*, **13**, 1066 (2023); https://doi.org/10.3390/nano13061066
9. S. Sharifi, H. Shakur, A. Mirzaei and M. Hosseini, *Int. Nanosci. Nanotechnol.*, **9**, 51 (2013).
10. J.C. Selvakumari, M. Ahila, M. Malligavathy and D.P. Padiyan, *Int. J. Miner. Metall. Mater.*, **24**, 1043 (2017); https://doi.org/10.1007/s12613-017-1494-2
11. I. Bibi, N. Nazar, M. Iqbal, S. Kamal, H. Nawaz, S. Nouren, Y. Safa, K. Jilani, M. Sultan and S. Ata, *Adv. Powder Technol.*, **28**, 2035 (2017); https://doi.org/10.1016/j.apt.2017.05.008
12. H. Hou, B. Mahdavi, S. Paydarfard, M.M. Zangeneh, A. Zangeneh, N. Sadeghian, P. Taslimi, V. Erduran and F. Sen, *Sci. Rep.*, **10**, 12195 (2020); https://doi.org/10.1038/s41598-020-68951-x2020
13. A.D. Dwivedi and K. Gopal, *Colloids Surf. A Physicochem. Eng. Asp.*, **369**, 27 (2010); https://doi.org/10.1016/j.colsurfa.2010.07.020
14. S. Iravani and R.S. Varma, *Green Chem.*, **22**, 2643 (2020); https://doi.org/10.1039/D0GC00885K
15. J. Singh, T. Dutta, K.-H. Kim, M. Rawat, P. Samddar and P. Kumar, *J. Nanobiotechnology*, **16**, 84 (2018); https://doi.org/10.1186/s12951-018-0408-4
16. A. Vennela, D. Mangalaraj, N. Muthukumarasamy, S. Agilan and K. Hemalatha, *Int. J. Electrochem. Sci.*, **14**, 3535 (2019); https://doi.org/10.20964/2019.04.40
17. V.D. Dang, N.T.H. Nhung, I. Rabani, N.T. Tran, B.T.P. Thuy and H.B. Truong, *RSC Adv.*, **15**, 19088 (2025); https://doi.org/10.1039/D5RA02705E
18. A. Kaur, S. Kumar, H. Kaur, G.S. Lotey, P.P. Singh, G. Singh, S. Kumar, J. Dalal, G. Bouzid, M. Misra, R. Pandey and S. Kaushal, *Mater. Adv.*, **5**, 8111 (2024); https://doi.org/10.1039/D4MA00795F
19. A. Chauhan, R. Kumar, S. Devi, Sonu, P. Raizada, V.K. Ponnusamy, P. Singh, A. Sudhaik, A.K. Mishra and R. Selvasembian, *Surf. Interfaces*, **54**, 105152 (2024); https://doi.org/10.1016/j.surfin.2024.105152
20. A. Diallo, A. Beye, T.B. Doyle, E. Park and M. Maaza, *Green Chem. Lett. Rev.*, **8**, 30 (2015); https://doi.org/10.1080/17518253.2015.1082646
21. N. Akhter, A. Liaquat, F. Murtaza, A. Yaqoob, S. Sharif, N. Jummah, M.I. Khan, A. Shanableh, L.G. Voskressensky and R. Luque, *Results Chem.*, **14**, 102151 (2025); https://doi.org/10.1016/j.rechem.2025.102151
22. M. Sivachidambaram, J.J. Vijaya, K. Kaviyarasu, L.J. Kennedy, H.A. Al-Lohedan and R.J. Ramalingam, *RSC Adv.*, **7**, 38861 (2017); https://doi.org/10.1039/C7RA06996K
23. J. Sharma, P. Srivastava, G. Singh, M.S. Akhtar and S. Ameen, *Mater. Sci. Eng. B*, **193**, 181 (2015); https://doi.org/10.1016/j.mseb.2014.12.012
24. N.O.M. Dewi, Y. Yulizar and D.O.B. Apriandanu, *IOP Conf. Ser.: Mater. Sci. Eng.*, **509**, 012105 (2019); https://doi.org/10.1088/1757-899X/509/1/012105
25. P. Chelliah, S.M. Wabaidur, H.P. Sharma, M.J. Jweeg, H.S. Majdi, M.M.R.A.L. Kubaisy, A. Iqbal and W.-C. Lai, *Water*, **15**, 910 (2023); https://doi.org/10.3390/w15050910
26. M. Saeed, N. Akram, S.A.R. Naqvi, M. Usman, M.A. Abbas, M. Adeel and A. Nisar, *Green Process. Synth.*, **8**, 382 (2019); https://doi.org/10.1515/gps-2019-0005
27. Y. Yulizar, D. O. B. Apriandanu and Y. Pratiwi, *IOP Conf. Ser.: Mater. Sci. Eng.*, **763**, 012022 (2020); https://doi.org/10.1088/1757-899X/509/1/012105
28. M.E.A. Sakib, M.L. Hasan, H. Roy, M.M. Hasan and M.M. Ali, *Next Nanotechnol.*, **8**, 100215 (2025); https://doi.org/10.1016/j.nxnano.2025.100215
29. M. Hafeez, R. Shaheen, B. Akram, S. Haq, S. Mahsud, S. Ali and R.T. Khan, *Mater. Res. Express*, **7**, 025019 (2020); https://doi.org/10.1088/2053-1591/ab70dd
30. M. Pudukudy and Z. Yaakob, *Chem. Pap.*, **68**, 1087 (2014); https://doi.org/10.2478/s11696-014-0561-7
31. R. Manigandan, K. Giribabu, R. Suresh, L. Vijayalakshmi, A. Stephen and V. Narayanan, *Chem. Sci. Trans.*, **2**, 47 (2013).
32. L. Estepa and M. Daudon, *Biospectroscopy*, **3**, 347 (1997); https://doi.org/10.1002/(SICI)1520-6343(1997)3:5<347::AID-BSPY3>3.0.CO;2-#
33. S.-H. Wu and D.-H. Chen, *J. Colloid Interface Sci.*, **259**, 282 (2003); https://doi.org/10.1016/S0021-9797(02)00135-2
34. P.G. Leles, M.A. Nascimento, J.C. Cruz, P.V.F. Sousa and R.P. Lopes, *Quím. Nova*, **42**, 497 (2019); https://doi.org/10.21577/0100-4042.20170363
35. J.K. Sharma, M.S. Akhtar, S. Ameen, P. Srivastava and G. Singh, *J. Alloys Compd.*, **632**, 321 (2015); https://doi.org/10.1016/j.jallcom.2015.01.172
36. S.D. Karse and M.C. Fite, *Physica B*, **689**, 416181 (2024); https://doi.org/10.1016/j.physb.2024.416181
37. C. Sahoo and A. Gupta, *J. Hazard. Mater.*, **215**, 302 (2012); https://doi.org/10.1016/j.jhazmat.2012.02.072
38. S. Dhiman and B. Gupta, *Environ. Technol. Innov.*, **23**, 101765 (2021); https://doi.org/10.1016/j.eti.2021.101765
39. R.J. Tayade, T.S. Natarajan and H.C. Bajaj, *Ind. Eng. Chem. Res.*, **48**, 10262 (2009); https://doi.org/10.1021/ie9012437